metals

MDPI

Article

Hot Deformation Behavior and Microstructural Evolution Characteristics of Ti-44Al-5V-1Cr Alloy Containing (γ + α_2 + B2) Phases

Hongwu Liu [1,2], Rong Rong [1], Fan Gao [2], Zhenxi Li [2], Yanguo Liu [3] and Qingfeng Wang [1,4,*]

1 State Key Laboratory of Metastable Materials Science and Technology, Yanshan University, Qinhuangdao 066004, China; liuhongwu0335@163.com (H.L.); rongrong@husun.com.cn (R.R.)
2 Titanium Alloys Laboratory, Beijing Institute of Aeronautical Materials, Beijing 100095, China; gfaoan@hotmail.com (F.G.); 13641145387@163.com (Z.L.)
3 School of Resources and Materials, Northeastern University at Qinhuangdao, Qinhuangdao 066004, China; ygliu93@163.com
4 National Engineering Research Center for Equipment and Technology of Cold Strip Rolling, Yanshan University, Qinhuangdao 066004, China
* Correspondence: wqf67@ysu.edu.cn; Tel.: +86-335-2039-067

Academic Editor: Hugo F. Lopez
Received: 17 October 2016; Accepted: 25 November 2016; Published: 2 December 2016

Abstract: The hot deformation behavior and microstructural evolution of Ti-44Al-5V-1Cr alloy were investigated by hot compression tests at temperatures of 1000–1250 °C and strain rates of 0.001–1 s^{-1}. It was indicated that the dependence of peak stress on deformation temperature and strain rate could be accurately described by a hyperbolic sine type equation. The activation energy, Q, was estimated to be 632 kJ/mol. The hot processing map was developed at different strains on the basis of dynamic materials modeling and the Murty criteria. As a result, the instability zones occurred in the regions of low temperature (<1050 °C) and a high strain rate (>0.1 s^{-1}). The flow soft mechanism of the instability regions is stress relaxation caused by localization deformation at lamellar boundaries. Dynamic recrystallization is the mainly refining and spheroidizing mechanism of lamellar microstructures. The optimum hot working condition of as-cast TiAl alloy occurs in the temperature range of 1175–1225 °C and the strain rate range 0.05–0.1 s^{-1}. The large-size TiAl alloy rectangular bars with crack-free appearance were successfully prepared by hot extrusion. After annealing, the fine and uniform microstructure with excellent deformation ability was obtained.

Keywords: TiAl alloy; hot deformation behavior; microstructure; dynamic recrystallization; hot extrusion

1. Introduction

Structure weight reducing is an important development direction of aeronautics and astronautics aircrafts. The novel lightweight and heat resisting structural material is urgently demanded. TiAl alloy is expected to become a substitute for nickel-based superalloys in several high temperature applications because of its low density, high strength, and excellent high temperature performance, and the working temperature could be up to 650–800 °C [1,2]. However, due to its poor ductility and narrow thermal processing window, the production of large-size and high-quality TiAl components from ingot material presents significant difficulties [3]. The application of TiAl alloy is limited. TiAl alloys containing the β phase show much better hot workability than (γ + α_2) TiAl alloys, even enabling the production of TiAl components using near conventional hot-working processes and equipment [2,4]. This increases the economic feasibility of hot processing for the manufacture of TiAl components.

For the γ phase, the α/α_2 (α_2 is low-temperature ordered α) phase, and the β/B2 (B2 is low-temperature ordered β) phase coexistence, the microstructural evolution of β phase containing TiAl alloy is very complex. During hot deformation, work hardening, dynamic recovery (DRV), dynamic recrystallization (DRX), and phase transformations often occur. Some works are available on the hot deformation behavior and microstructural evolution of β phase containing TiAl, and the compositions therein are Ti-43.5Al-4Nb-1Mo-0.1B [5], Ti-43Al-2Cr-2Mn-0.2Y [6], Ti-43Al-4Nb-1.4W-0.6B-0.2Y [7], and Ti-45Al-7Nb-0.4W-0.15B [8,9]. The lamellar grain sizes of these alloys were all fine because of β-phase solidification and the addition of Band/or Y elements. However, until the present, the hot deformation behavior and microstructural evolution of multi-phase TiAl alloys without the addition of B and/or Y have rarely been reported. Without the addition of the grain refinement elements B and Y, the lamellar grain sizes of TiAl ingots would be coarse. Seetharaman and his co-workers [10] suggested that the plastic flow behavior and microstructural evolution showed a very strong dependence on the lamellar grain size. It is known that the critical stress concentration to create a micro-crack is closely related with the grain size of the alloy. Therefore, the hot deformation of the coarse microstructure must be difficult.

The essential aim of the present study was to explore the hot deformation behavior and microstructural evolution of large ingot size Ti-44Al-5V-1Cr alloy, to establish a constructive relationship and a hot processing map, and, using the optimized parameters, to breakdown the coarse grains of the ingot.

2. Materials and Methods

A large-size ingot of Ti-44Al-5V-1Cr (atom %) was melted three times by vacuum arc melting furnace using sponge Ti (99.9%), purity Al (99.99%), Al-V inter-alloy, and granular Cr (99.9%). The final ingot size was Φ220 mm × 750 mm. Hot compression tests were performed on a Thermecmastor-Z machine (Fuji Electronics Industry, Osaka, Japan) at 1000–1250 °C with strain rates of 0.001–1 s^{-1} to obtain the true strain-stress curves. Cylindrical specimens with the dimension of Φ8 mm × 12 mm were machined by electro-discharge machining and mechanical grinding methods. Tantalum foils were employed as a lubricant to minimize the friction during the tests. Each specimen was heated to the deformation temperature at a rate of 5 °C/s, soaked for 5 min, compressed to an engineering strain of 50% (true strain of 0.7), and then quenched immediately to preserve the as-deformed microstructure. Furthermore, a large-scale engineering extrusion was conducted to verify the optimal process proposed based on thermal physical simulation. The ingot was machined into cylindrical billet with dimensions of Φ192 mm × 210 mm and canned by 304 stainless steel. Finally, hot-canned extrusion was conducted using the optimum process proposed later in this paper.

The initial and deformed microstructures were characterized by optical microscopy (OM, Lecia DMI3000 M, Leica Microsystems, Wetzlar, Germany), scanning electron microscopy (SEM, JSM-7001F, JEOL, Tokyo, Japan) with a back-scattered electron (BSE) detector, electron back scattered diffraction (EBSD, EDAX, Mahwah, NJ, USA),and transmission electron microscopy (TEM, FEI Tecnai G2 F20, FEI Company, Hillsboro, OR, USA). Phase analyses were conducted by X-ray diffraction (XRD, ULTIMA IV, Rigaku Corporation, Tokyo, Japan). For optical metallographic examination, the samples were mechanically polished and etched in a solution of 5% HF, 10% HNO_3, and 85% H_2O. Samples for SEM observation were prepared by mechanical polishing.The foils for TEM were prepared by hand grinding to a thickness of 50 μm and then thinned using a twin-jet technique in the electrolyte of 6% $HClO_4$-35% *N*-butanol-59% methanol at 15 V and −30 °C. The EBSD samples were electro-polished in the same electrolyte as the twin-jet, and the collected EBSD data were interpreted with TSL OIM 6.0 analysis software (EDAX, Mahwah, NJ, USA).

3. Results and Discussion

3.1. As-Cast Microstructure

Figure 1 presents the XRD pattern of the as-cast Ti-44Al-5V-1Cr alloy, and the pattern indicates that the TiAl alloy consisted of the three major phases: γ phase, α_2 phase, and B2 phase. It can be seen from Figure 2 that the as-cast microstructure was mainly composed of (α_2 + γ) lamellar colonies, equiaxed γ grains (dark contrast), and irregular B2 grains (white contrast). The mixture of γ grains and B2 existing along the colony boundaries and inside the colonies, was produced by the discontinuous reaction of β/B2 → γ in the solidification processes [11]. For TiAl alloys, when the mole fraction of Al is less than 45%, it solidifies completely through the β phase field. The positive significance of this kind of TiAl alloy is its fine lamellar colony size. In this study, the mole fraction of Al is 44%; however, the size of the lamellar colony was still large and in the range of 400–1000 μm. This is mainly due to the large-size ingot and its high melting current and slow cooling rate, which cause the original beta grain size to increase during the solidification process. In addition, grain refinement elements, such as B and Y, are not included in the present alloy.

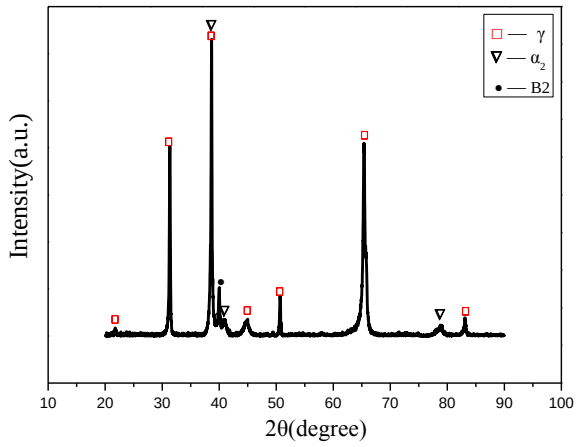

Figure 1. XRD pattern of the as-cast Ti-44Al-5V-1Cr alloy.

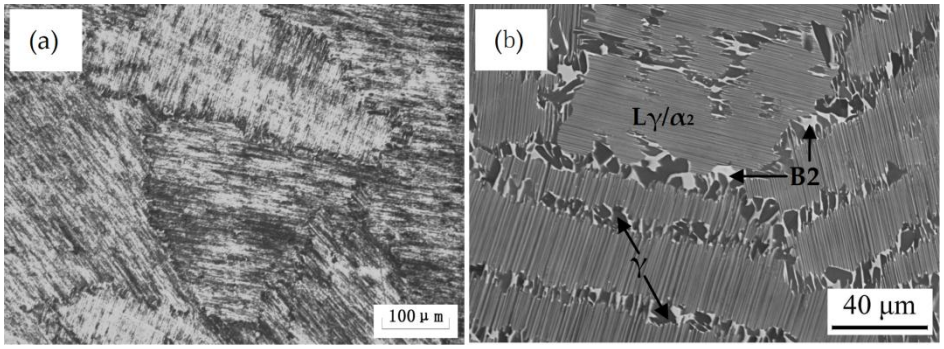

Figure 2. Original microstructure of as-cast Ti-44Al-5V-1Cr alloy: (**a**) OM; (**b**) SEM–BSE (bright—B2, dark—γ, grey—lamellae).

3.2. Flow Behavior and Constitutive Equation

The true strain-stress curves of large-size Ti-44Al-5V-1Cr alloy with different deformation conditions are shown in Figure 3. Obviously, the flow stress is very sensitive to temperature and strain rate. With increasing temperature and decreasing strain rate, the stress decreases. Generally, a constant flow-stress is associated with the occurrence of DRV, while a single-peak flow curve is indicative of DRX, according to [12]. The present steady-state type curves of the as-extruded

Ti-44Al-5V-1Cr alloy deformed at 1250 °C and $\leq$0.01 s^{-1} imply that DRV was the mechanism for softening. The other curves exhibited peak stress at the initial deformation stage, which decreased gradually to a steady state with increasing strain, inferring a mechanism of softening controlled by DRX and cracks. In this work, however, the cracks occurred in samples compressed under extensive conditions, due to the coarse-grained microstructure of as-cast alloy, and these cracks may have resulted in an additional reduction of flow stress. The flow softening of TiAl alloys might also be caused by adiabatic heating, flow localization, kinking, or reorientation of lamellae during deformation [13]. The mechanism for deformation softening of the as-cast Ti-44Al-5V-1Cr alloy needs to be further analyzed via microstructural observation.

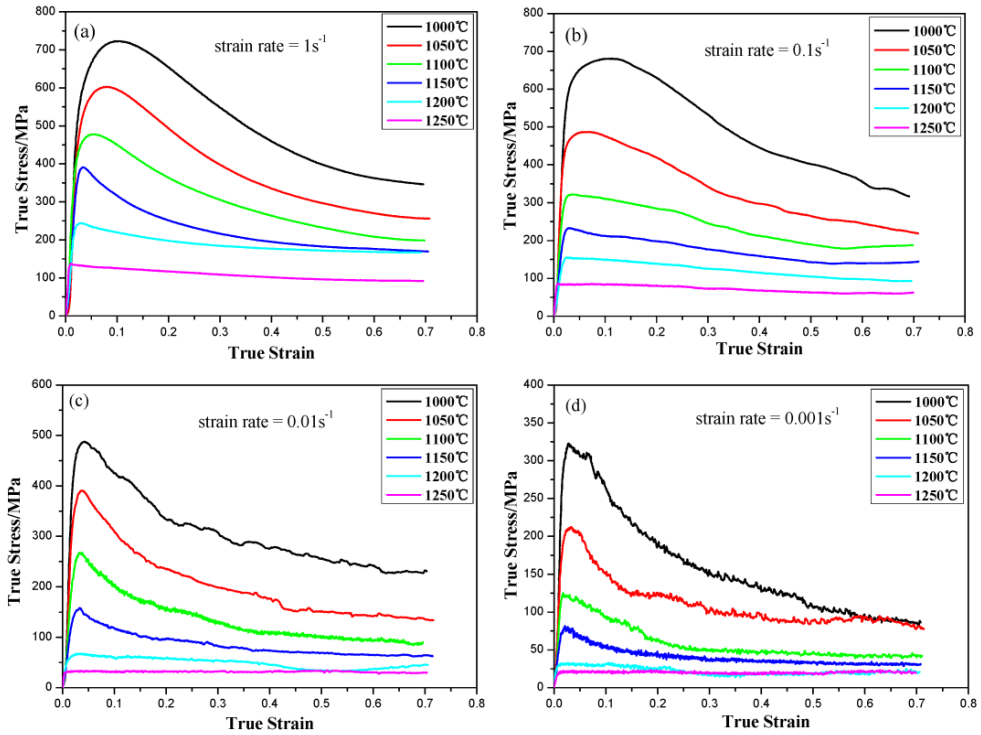

Figure 3. True stress-strain curves of large-size Ti-44Al-5V-1Cr alloy under different strain rates: (**a**) 1 s^{-1}; (**b**) 0.1 s^{-1}; (**c**) 0.01 s^{-1}; (**d**) 0.001 s^{-1}.

To describe the relationship between the flow stress and the deformation parameters, a constitutive equation was proposed by Sellars et al. [14,15]. It considers the flow behavior of materials during deformation as a thermally activated process and is expressed as

$$Z = \dot{\varepsilon}\exp\left(Q/RT\right) = A\left[\sin h(\alpha\sigma)\right]^{n} \quad (1)$$

where Z is the Zener-Hollomon parameter, $\dot{\varepsilon}$ is the strain rate, σ is the flow stress, Q is the apparent activation energy of deformation (kJ/mol), R is the molar gas constant (8.314 J/mol·K), T the deformation temperature (K), and A, n, and α material constants. The Q value can be calculated by a transformation of Equation (1):

$$Q = R\left\{\frac{\partial \ln\dot{\varepsilon}}{\partial \ln\left[\sin h(\alpha\sigma)\right]}\right\}_T \cdot \left\{\frac{\partial \ln\left[\sin h(\alpha\sigma)\right]}{\partial\left(1/T\right)}\right\}_{\dot{\varepsilon}} \quad (2)$$

Figure 4a–d shows the relationships of $\ln\dot{\varepsilon} - \sigma$, $\ln\dot{\varepsilon} - \ln\sigma$, $\ln\dot{\varepsilon} - \ln[\sin h(\alpha\sigma)]$, and $\ln[\sin h(\alpha\sigma)] - 10^4/T$ at peak stresses as well as their linear regression results. The activation energy of hot deformation for the large-size Ti-44Al-5V-1Cr alloy calculated from Figure 4 was 632 kJ/mol.

Equation (1) can also be expressed in logarithms as

$$\ln Z = \ln A + n \ln [\sin h(\alpha\sigma)] \tag{3}$$

By performing the linear fitting of $\ln Z - \ln [\sin h(\alpha\sigma)]$, as shown in Figure 4e, the values of n and A were found to be 3.4 and 8.95×10^{21}, respectively, with the values of intercept and slope taken in the curve. The constitutive equation was further determined as

$$\dot{\varepsilon} = 8.95 \times 10^{21} [\sin h(0.00454\sigma)]^{3.4} \exp(-632/RT) \tag{4}$$

The correlation coefficient, $R2$, for the constitutive model was 0.98, indicating that it had a high accuracy in describing the high temperature deformation behavior of the present material and can be used in analytical or computational modeling of hot working operations.

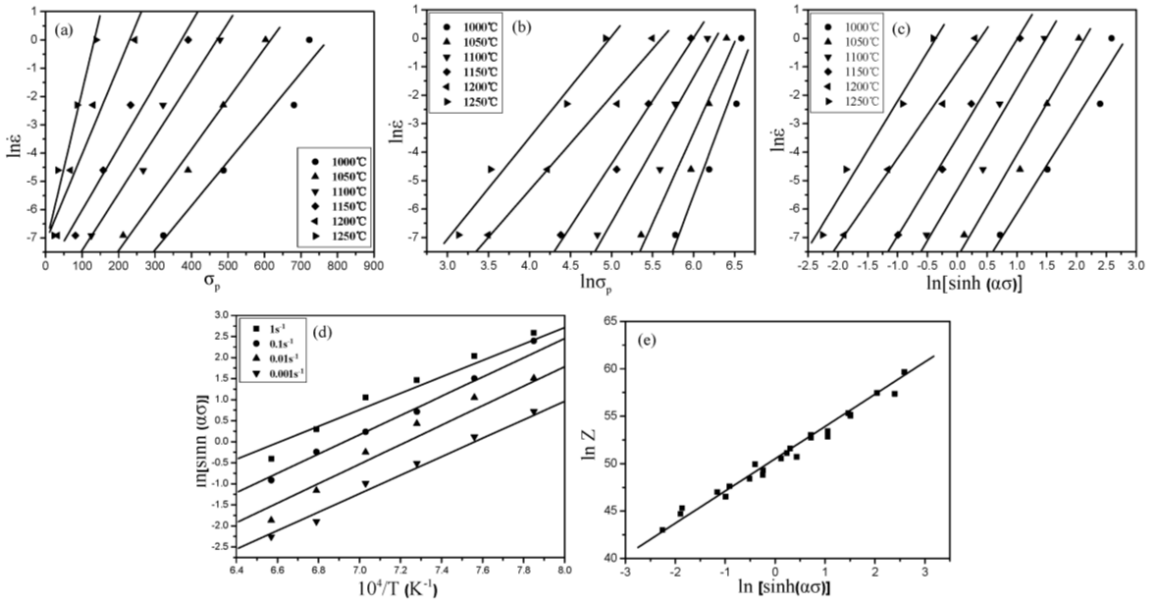

Figure 4. Relationship between peak stress, strain rate, temperature, and Z parameter: (**a**) $\ln\dot{\varepsilon}\sigma$; (**b**) $\ln\dot{\varepsilon} - \ln\sigma$; (**c**) $\ln\dot{\varepsilon} - \ln[\sin h(\alpha\sigma)]$; (**d**) $\ln[\sin h(\alpha\sigma)] - 10^4/T$; (**e**) $\ln Z - \ln[\sin h(\alpha\sigma)]$.

3.3. Hot Processing Map

Hot processing maps have been widely used to study deformation behaviors of many materials [5,16,17]. Processing maps are normally constructed by overprinting power dissipation maps and instability regime maps. Processing maps are based on the dynamic materials model, the principles of which have been described earlier [18–21]. It was claimed that the power for hot processing was consumed by changes in the shape and simultaneous microstructure of a workpiece.

The workpiece undergoing hot deformation is considered to be a dissipator of power and the total power dissipated instantaneously can be expressed as

$$P = \sigma\dot{\varepsilon} = \int_0^{\dot{\varepsilon}} \sigma d\dot{\varepsilon} + \int_0^{\sigma} \dot{\varepsilon}\, d\sigma = G + J \tag{5}$$

where G is the work function, and J is the power co-content. The strain rate sensitivity (m) of flow stress is the factor that partitions power between deformation heat and microstructural changes since

$$\frac{dJ}{dG} \approx \frac{\Delta \log\sigma}{\Delta \log\dot{\varepsilon}} = m \tag{6}$$

The efficiency of dissipation, η, represents a ratio of the power dissipation in a microstructural change to the total power. The evaluation of η has been carried out extensively by comparing the power dissipation from a microstructural change with an ideal dissipation. From the ratio of J and $J_{max} = P/2$, the efficiency of power dissipation η is given by

$$\eta = \frac{J}{J_{max}} = \frac{P - G}{P/2} \tag{7}$$

where η can take values between 0 and 1. The dependence of η on hot processing conditions, including temperature and strain rate, is finally described in a power dissipation map. G can be determined after the modified relation reported in [22]:

$$G = \left[\frac{\sigma\dot{\varepsilon}}{m+1}\right]_{\dot{\varepsilon}_{min}} + \int_{\dot{\varepsilon}_{min}}^{\dot{\varepsilon}} \sigma d\dot{\varepsilon} \tag{8}$$

As a generally valid instability criterion, the $D = J$ condition is used, where the power dissipation function D is set equal to metallurgical changes. Thereafter, the deformation instability region is expected to occur when

$$\frac{2m}{\eta} - 1 < 0 \tag{9}$$

The processing maps for the as-cast Ti-44Al-5V-1Cr alloy obtained in the temperature range of 1000–1250 °C and at the strain rate range of 0.001–1 s^{-1} at true strains of 0.2 and 0.6, through super imposing the instability maps on the power dissipation maps are shown in Figure 5. At relatively low temperatures (below 1050 °C) and in the high strain rate regime (above 0.1 s^{-1}), the dissipation efficiency was very low in all cases. The instability zone increased with the increase of the strain. The instability zones occurred in regions of low temperature and high strain rate (>0.1 s^{-1}), where the dissipation efficiency was less than 0.4. This suggests that the hot workability was not good in these regions. Generally, the maximum η represents the optimal processing window. In the map of a strain of 0.2 (Figure 5a), there was one domain showing a peak efficiency of 0.55. When the strain increased to the level of 0.6, the peak efficiency increased to 0.65. It was also noted that the peak efficiencies occurred at the same region at 1200 °C and 0.01 s^{-1}. The optimum hot working condition of large-size as-cast Ti-44Al-5V-1Cr alloy for all the true strains occurred in the temperature range of 1175–1225 °C and the strain rate range 0.05–0.1 s^{-1}, where the dissipation efficiency was more than 0.5.

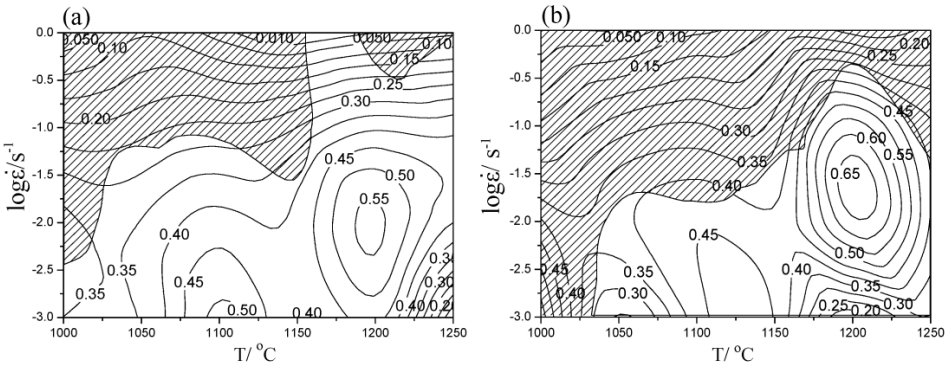

Figure 5. Hot processing maps at different true strains of as-cast Ti-44Al-5V-1Cr alloy. (**a**) The true strain is 0.2; (**b**) the true strain is 0.6. The contours represent efficiency of power dissipation. The shadow region corresponds to flow instability.

3.4. Microstructural Evolution

Figure 6 shows the typically deformed structures in the instability zone of Ti-44Al-5V-1Cr alloy. It can be seen that obvious localization deformation fracture occurred at the lamellar boundaries, and

the fracture angle basically followed an angle of 45° to the compressive axis. Cavities at the grain boundaries are considered to be caused by stress concentration, which is more liable to occur at grain boundaries and triple-junction points [23].For the samples deformed at 1050 °C/1 s^{-1} (Figure 6a) and 1150 °C/1 s^{-1} (Figure 6b), at high strain rates, this stress concentration cannot be relieved or accommodated by the dislocation motion, but by nucleation of cracks.

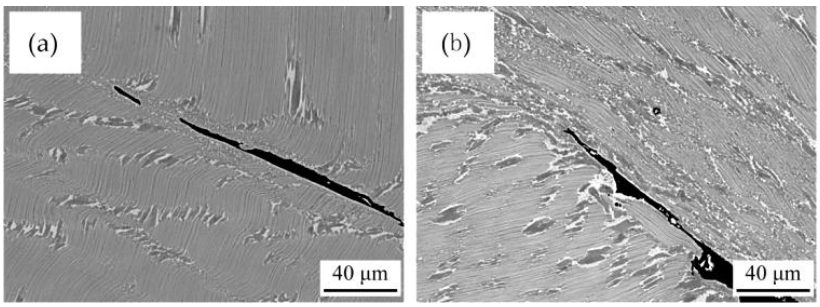

Figure 6. Observations of microstructure and flaw in as-cast Ti-44Al-5V-1Cr alloy samples deformed at (**a**) 1050 °C/1 s^{-1} and (**b**) 1150 °C/1 s^{-1}, typically in the instability zone.

Figure 7 shows SEM-BSE micrographs of the Ti-44Al-5V-1Cr alloy deformed to a 50% reduction (true strain = 0.7) in the safe deformation zones. At deformation conditions of 1050 °C and 0.01 s^{-1} (Figure 7a), the lamellar orientation was perpendicular to the direction of the compression axis, and dynamic recrystallization occurred initially in the lamellar boundaries and where the γ and B2 grains co-existed. The lamellae, which were surrounded by the mixture of gamma and B2, were easily rotated to the direction perpendicular to the compression axis under the action of pressure [8]. The soft B2 phase can promote lamellar colony boundary sliding and grain rotating effectively to release stress concentration and prevent premature fracture failure. As the temperature was increased to 1150 °C (Figure 7b,c), the residual lamellae decreased significantly, a large number of lamellar colonies decomposed into α and γ equiaxed grains; similarly, reducing the rate of deformation can effectively improve the equiaxed grain content. By comparing the deformed microstructure in differing deformation conditions, we found that the lamellar decomposition/globularization could be promoted evidently by increasing the temperature or decreasing the strain rate. The bright-field TEM images in Figure 8 reveal the microstructures after deformation at 1150 °C with a strain rate of 0.01 s^{-1}. The lamellar colonies bended and kinked heavily (Figure 8a), laths coarsened and decomposed partially in lamellar colonies (Figure 8b), and dynamically recrystallized grains are shown in Figure 8c. DRX is the main refining and spheroidizing mechanism of lamellar microstructures. The dislocations and twin deformation can be seen in Figure 8d,e. As demonstrated in [24,25], dislocation motion is achieved by both glide and climb, with the relative contributions depending on the deformation conditions. Dislocation climb often occurs at low stresses and strain rates. The deformation mechanism of the current TiAl alloy can be concluded as dislocation slip, dislocation climb, and mechanical twins, which induce the final dynamic recrystallization.

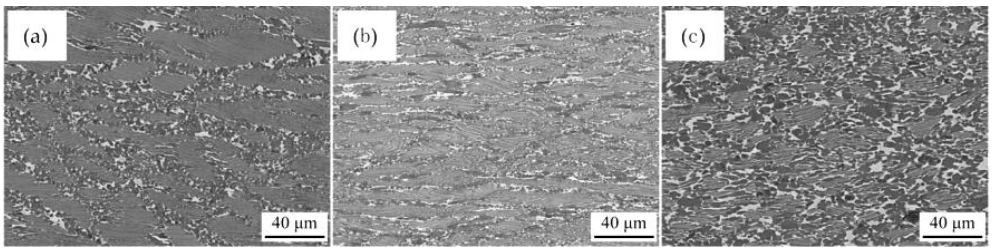

Figure 7. Observations of microstructure in as-cast Ti-44Al-5V-1Cr alloy sample deformed at (**a**) 1050 °C/0.01 s^{-1}, (**b**) 1150 °C/0.1 s^{-1}, and (**c**) 1150 °C/0.01 s^{-1}, typically in the safe zone.

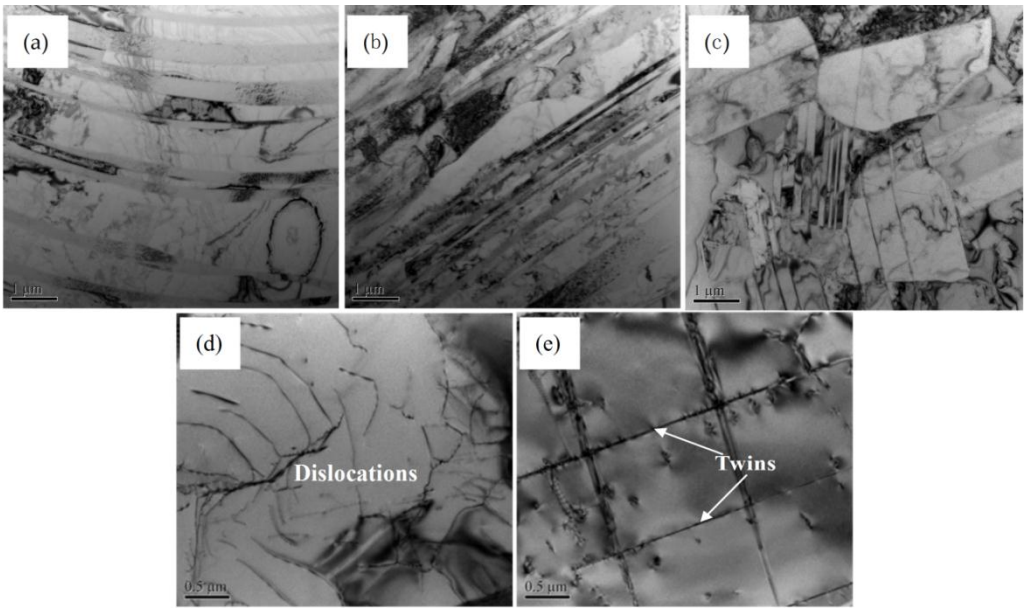

Figure 8. Bright-field TEM images showing (**a**) bending of lamellae; (**b**) laths coarsened and decomposed; (**c**) dynamically recrystallized grains; (**d**) dislocations; and (**e**) twins in γ grain after deformation at 1150 °C with a strain rate of 0.01 s^{-1}.

3.5. Large-Size TiAl Bars with Uniform and Fine Grains Produced by Hot Extrusion

Based on the analysis of the deformation mechanism under different deformation conditions, combined with the hot processing map and the actual hot extrusion process, the rectangular bars of Ti-44Al-5V-1Cr alloy with crack-free appearance were successfully prepared at 1200 °C, and the extrusion ratio was 3, as shown in Figure 9a. The dimensions of the Ti-44Al-5V-1Cr alloy rectangular bars were 165 mm × 85 mm × 410 mm. Figure 9b shows that the bars consisted of a majority of remnant γ/α_2 lamellar and a certain amount of DRX grains.

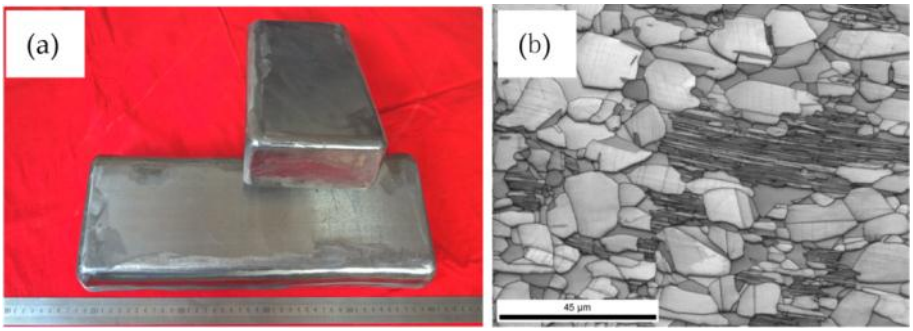

Figure 9. The large-sizeTi-44Al-5V-1Cr alloy rectangular bars produced by hot extrusion. (**a**) The appearance of TiAl alloy bars; (**b**) IQ map of the as-extruded microstructure.

In order to obtain a uniform microstructure, the as-extruded bars were annealed at 1150 °C and held on 6 h. Microstructure observations of as-annealed alloy were shown in Figure 10. Figure 10a shows that the microstructure consisted of uniform and fine grains, and remnant lamellar colonies were nonexistent. The grain size distribution map (Figure 10b) shows that the average grain size was about 9.7 μm. The phase map obtained by EBSD (Figure 10c) shows that the fractions of γ, α_2, and B2 were 73.0%, 10.6%, and 16.5%, respectively. This kind of microstructure has excellent hot deformability.

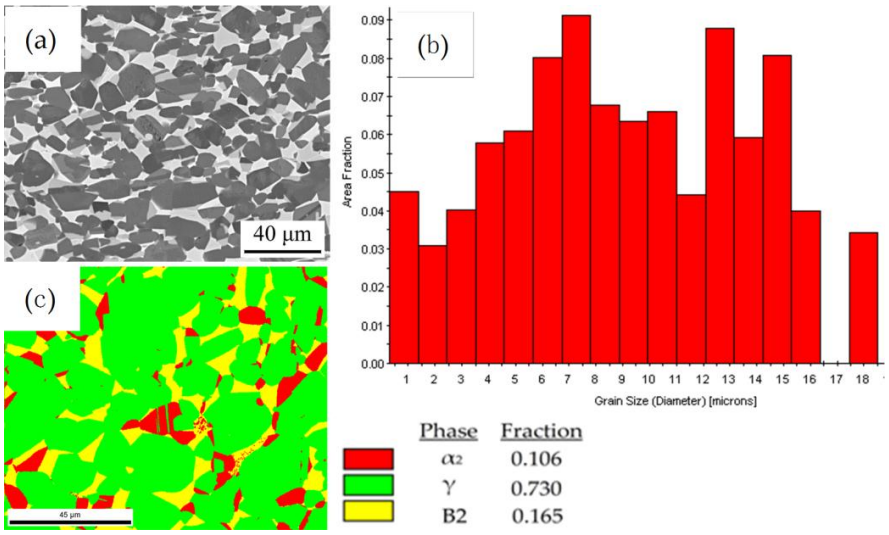

Figure 10. Microstructure observations of as-extruded alloy annealed at 1150 °C and held on 6 h. (**a**) SEM-BSE image; (**b**) grain size distribution map; and (**c**) phase map by EBSD.

4. Conclusions

The hot deformation behavior and microstructural evolution characteristics of a large-size β phase containing Ti-44Al-5V-1Cr alloy were investigated. The following conclusions are drawn based on the aforementioned results:

(1) The flow stress of the large-size Ti-44Al-5V-1Cr alloy increased with increasing strain rate and decreasing deformation temperature. The interrelations of peak flow stress, strain rate and deformation temperature can be described by the Arrhenius equation modified by a hyperbolic sine function. The activation energy was determined to be 632 kJ/mol and a constitution equation was built as:

$$\dot{\varepsilon} = 8.95 \times 10^{21} \left[\sin h(0.00454\sigma)\right]^{3.4} \exp\left(-632/RT\right) \quad (10)$$

(2) The hot processing map is developed at the strains of 0.2 and 0.6 for the as-cast TiAl alloy. The instability zones occurred in the regions of low temperature and high strain rate (>0.1 s^{-1}). The flow soft mechanism of the instability regions is stress relaxation caused by localization deformation at lamellar boundaries.

(3) The optimum hot working condition of large-size as-cast Ti-44Al-5V-1Cr alloy for all the true strains occurs in the temperature range of 1175–1225 °C and the strain rate range 0.05–0.1 s^{-1}. Dynamic recrystallization is the mainly refining and spheroidizing mechanism of lamellar microstructures.

(4) The large-size Ti-44Al-5V-1Cr alloy rectangular bars with crack-free appearance were successfully prepared by hot extrusion. After annealing, the fine and uniform microstructure with excellent deformation ability was obtained.

Acknowledgments: This work was supported by the National Key Research and Development Program of China (Grant No. 2016YFB0301203), the Natural Science Foundation of Hebei Province (Grant No. E2014501129), and the Aviation Science Foundation of China (Grant No.2014E62149R).

Author Contributions: Qingfeng Wang designed the experiments; Hongwu Liu, Rong Rong, and Fan Gao performed the experimental work; Hongwu Liu, Yanguo Liu, and Zhenxi Li analyzed the data; Hongwu Liu and Qingfeng Wang contributed to the writing and editing of the manuscript.

Conflicts of Interest: The authors declare no conflict of interest.

References

1. Yamaguchi, M.; Inui, H.; Ito, K. High-temperature structural intermetallics. *Acta Mater.* **2000**, *48*, 307–322. [CrossRef]

2. Clemens, H.; Mayer, S. Design, Processing, Microstructure, Properties, and Applications of Advanced Intermetallic TiAl Alloys. *Adv. Eng. Mater.* **2013**, *15*, 191–215. [CrossRef]
3. Paul, J.D.H.; Lorenz, U.; Oehring, M.; Appel, F. Up-scaling the size of TiAl components made via ingot metallurgy. *Intermetallics* **2013**, *32*, 318–328. [CrossRef]
4. Tetsui, T.; Shindo, K.; Kaji, S.; Kobayashi, S.; Takeyama, M. Fabrication of TiAl components by means of hot forging and machining. *Intermetallics* **2005**, *13*, 971–978. [CrossRef]
5. Schwaighofer, E.; Clemens, H.; Lindemann, J.; Stark, A.; Mayer, S. Hot-working behavior of an advanced intermetallic multi-phase γ-TiAl based alloy. *Mater. Sci. Eng. A* **2014**, *614*, 297–310. [CrossRef]
6. Cui, N.; Kong, F.; Wang, X.; Chen, Y.; Zhou, H. Microstructural evolution, hot workability, and mechanical properties of Ti-43Al-2Cr-2Mn-0.2Y alloy. *Mater. Des.* **2016**, *89*, 1020–1027. [CrossRef]
7. Wang, Y.; Liu, Y.; Yang, G.Y.; Li, J.B.; Liu, B.; Wang, J.W.; Li, H.Z. Hot deformation behaviors of β phase containing Ti-43Al-4Nb-1.4W-based alloy. *Mater. Sci. Eng. A* **2013**, *577*, 210–217. [CrossRef]
8. Liu, B.; Liu, Y.; Li, Y.P.; Zhang, W.; Chiba, A. Thermomechanical characterization of β-stabilized Ti-45Al-7Nb-0.4W-0.15B alloy. *Intermetallics* **2011**, *19*, 1184–1190. [CrossRef]
9. Liu, B.; Liu, Y.; Huang, L.; Li, H.; He, Y. Characterization of phase transformation during hot compressive deformation in a β-stabilized Ti-45Al-7Nb-0.4W-0.15B alloy. *Mater. Charact.* **2015**, *105*, 113–117. [CrossRef]
10. Seetharaman, V.; Semiatin, S.L. Effect of the lamellar grain size on plastic flow behavior and microstructure evolution during hot working of a gamma titanium aluminide alloy. *Metall. Mater. Trans. A* **2002**, *33*, 3817–3830. [CrossRef]
11. Niu, H.Z.; Chen, Y.Y.; Xiao, S.L.; Xu, L.J. Microstructure evolution and mechanical properties of a novel beta γ-TiAl alloy. *Intermetallics* **2012**, *31*, 225–231. [CrossRef]
12. Sakai, T.; Belyakov, A.; Kaibyshev, R.; Miura, H.; Jonas, J.J. Dynamic and post-dynamic recrystallization under hot, cold and severe plastic deformation conditions. *Prog. Mater. Sci.* **2014**, *60*, 130–207. [CrossRef]
13. Kim, J.H.; Chang, Y.W.; Lee, C.S.; Ha, T.K. High-temperature deformation behavior of a gamma TiAl alloy—Microstructural evolution and mechanisms. *Metall. Mater. Trans. A* **2003**, *34*, 2165. [CrossRef]
14. Sellars, C.M.; McTegart, W.J. On the mechanism of hot deformation. *Acta Met.* **1966**, *14*, 1136–1138. [CrossRef]
15. Jonas, J.J.; Sellars, C.M.; Tegart, W.J.M. Strength and structure under hot-working conditions. *Metall. Rev.* **1969**, *14*, 1–24. [CrossRef]
16. Sun, C.; Xiang, Y.; Zhou, Q.; Politis, D.J.; Sun, Z.; Wang, M. Dynamic Recrystallization and Hot Workability of 316LN Stainless Steel. *Metals* **2016**, *6*, 152. [CrossRef]
17. Sun, C.; Zuo, X.; Xiang, Y.; Yang, J. Investigation on Hot Deformation Behavior and Hot Processing Map of BSTMUF601 Super-Alloy. *Metals* **2016**, *6*, 70. [CrossRef]
18. Jonas, J.J.; Holt, R.A.; Coleman, C.E. Plastic stability in tension and compression. *Acta Metall.* **1976**, *24*, 911–918. [CrossRef]
19. Raj, R. Development of a Processing Map for Use in Warm-Forming and Hot-Forming Processes. *Metall. Trans. A* **1981**, *12*, 1089–1097. [CrossRef]
20. Montheillet, F.; Jonas, J.J.; Neale, K.W. Modeling of dynamic material behavior: A critical evaluation of the dissipator power co-content approach. *Metall. Mater. Trans. A* **1996**, *27*, 232–235. [CrossRef]
21. Prasad, Y.V.R.K.; Seshacharyulu, T. Modelling of hot deformation for microstructural control. *Int. Mater. Rev.* **1998**, *43*, 243–258. [CrossRef]
22. Murty, S.V.S.N.; Rao, B.N. Ziegler's Criterion on the Instability Regions in Processing Maps. *J. Mater. Sci. Lett.* **1998**, *17*, 1203–1205. [CrossRef]
23. Dao, M.; Kad, B.K.; Asaro, R.J. Deformation and fracture under compressive loading in lamellar TiAl microstructures. *Philos. Mag. A* **1996**, *74*, 569–591. [CrossRef]
24. Appel, F. Diffusion assisted dislocation climb in intermetallic gamma TiAl. *Mater. Sci. Eng. A* **2001**, *317*, 115–127. [CrossRef]
25. Imayev, R.M.; Imayev, V.M.; Oehring, M.; Appel, F. Microstructural evolution during hot working of Ti aluminide alloys: Influence of phase constitution and initial casting texture. *Metall. Mater. Trans. A* **2005**, *36*, 859–867. [CrossRef]